# Biological characteristics of two pathogens causing brown blotch in *Agaricus Bisporus* and the toxin identification of *Cedecea neteri*

Zaixing Huang[1] , Yiyun Huang[1], Yulu Nie[1] and Bin Liu[1,2*]

## Abstract

Brown blotch disease in *Agaricus bisporus* reduces its commercial value, resulting in significant economic losses. The pathogens of brown blotch disease are diverse. Current research on the biological characteristics and toxins has been limited to *Pseudomonas tolaasii* but lacks understanding of other pathogens. Understanding the biological characteristics of the pathogens and identifying their toxins are essential prerequisites for disease prevention and control. This study isolated two pathogens from brown discoloration in *A. bisporus* in Guangxi, China, and identified them as *Pseudomonas tolaasii* and *Cedecea neteri*. *C. neteri* exhibited stronger resistance to sodium dodecyl sulfate (SDS) and $H_2O_2$ and a broader pH adaptation range than *P. tolaasii*. *P. tolaasii* showed higher swimming motility than *C. neteri*. *C. neteri* produces two toxins identified as phenylacetic acid and p-hydroxybenzoic acid, causing browning symptoms in *A. bisporus* at 20 μg and 10 μg, respectively. The present study compared various biological characteristics between *P. tolaasii* and *C. neteri*. The toxins produced by *C. neteri* were extracted and identified, and their toxicity to *A. bisporus* was evaluated, which is the first report on *C. neteri* toxins. These discoveries have enhanced our understanding of the biological characteristics and biotoxins of *C. neteri*. The research findings offer new insights for developing novel disease prevention and control strategies.

**Keywords** *Agaricus bisporus*, Bacterial disease, *Pseudomonas tolaasii*, *Cedecea neteri*, Toxin, Biological characteristics

## Background

*Agaricus bisporus*, a widely cultivated edible and medicinal fungus, accounts for 15% of global mushroom production. It is rich in nutrients and contains various bioactive substances and trace elements, making significant contributions to the food industry and human health (Ramos et al. 2019; Mleczek et al. 2020). However, the production of *A. bisporus* is susceptible to invasion by pathogens, including fungi, bacteria, and viruses, which leads to severe economic losses. In particular, bacterial blotch disease has caused significant losses to the commercial value and yield of *A. bisporus*. *Pseudomonas tolaasii* is considered to be the most dominant or destructive pathogen in *A. bisporus* production, causing brown blotch disease (Tajalipour et al. 2014). *P. tolaasii* produces a lipopeptide consisting of 18 amino acids, called tolaasin, which is the main pathogenic toxin and causes the lesion-symptom same as direct inoculation with *P. tolaasii* suspensions on *A. bisporus* (Osdaghi et al. 2019). The occurrence patterns, prevention and control strategies of *P. tolaasii*, as well as the molecular structure, action mechanism, and related gene functions of tolaasin, have been comparatively well-studied (Soler-Rivas et al. 1999; Taparia et al. 2021).

*Correspondence:
Bin Liu
liubin@gxu.edu.cn
[1] Institute of Applied Microbiology, College of Agriculture, Guangxi University, Nanning 530005, China
[2] Guangxi Key Laboratory for Agro-Environment and Agro-Product Safety, Nanning 530005, China

With increasing attention from researchers to the pathogenicity of *A. bisporus*, an increasing number of bacterial pathogens have been discovered. For instance, *Cedecea neteri* was first confirmed as the pathogen causing brown blotch disease in *A. bisporus* in Iran in 2022, with an infection rate as high as 20% (Hamidizade et al. 2022). Additionally, *P. agarici* (Cantore and Iacobellis 2004), *Mycetocola* sp. (Hamidizade et al. 2020), and others can also induce brown blotch disease in *A. bisporus* (Taparia et al. 2020, 2021). Thus, the pathogens responsible for brown blotch disease in *A. bisporus* are diverse.

*C. neteri* has a wide host range and high disease incidence. For example, it can cause yellow rot disease on *Pleurotus pulmonarius* with an incidence of more than 10% (Liu et al. 2021), soft rot disease on *Pholiota nameko* with an incidence over 20% (Yan et al. 2018), and yellow sticky disease of *Flammulina velutipes* (Yan et al. 2019). This evidence indicates that *C. neteri* may have a high disease incidence in *A. bisporus* and other edible fungi. Furthermore, it is an opportunistic pathogen for humans (Thompson and Sharkady 2021; Sharkady et al. 2023). Therefore, *C. neteri* poses a significant threat to mushroom cultivation and human health, and we must pay attention to its damage.

Understanding the structure of pathogenic virulence factors will enable us to target them to control bacterial blotch disease in mushrooms. For instance, certain food additives can interact with the toxin tolaasin produced by *P. tolaasii*, known as tolaasin-inhibitory factors (TIFs) (Yun et al. 2017). These TIFs can suppress both the brown blotch disease caused by *P. tolaasii* and the activity of tolaasin on mycelial membranes (Park et al. 2010; Yun et al. 2017). The application of TIFs in the prevention and control of mushroom brown blotch disease shows promising prospects and toxin-based control strategies have emerged as a new direction in managing mushroom diseases (Park et al. 2010; Yun et al. 2023). However, we only know that *Cedecea* sp. can produce a small amount of siderophore (Yuan et al. 2022). There is no research on toxins produced by *Cedecea* sp. acting on fungi or plants, and the biological characteristics of *C. neteri* remain poorly understood, limiting our knowledge about this organism.

From 2020 to 2022, we collected brown blotch samples from various *A. bisporus* production sites in Guangxi and isolated pathogens. This study investigated the pathogenic-related biological characteristics of *P. tolaasii* and *C. neteri*. We purified the toxin from the ethyl acetate fraction of the *C. neteri* fermentation broth by thin-layer chromatography (TLC), silica gel column chromatography (SGCC), and high-performance liquid chromatography (HPLC), and determined the molecular structure of the toxin based on their nuclear magnetic resonance (NMR) and mass spectrometry (MS). We evaluated the toxicity of the toxin on the *A. bisporus* fruiting body. This study aimed to elucidate the biological characteristics of *P. tolaasii* and *C. neteri* and the toxin produced by *C. neteri*, providing a basis for the development of accurate and environmentally friendly prevention and control strategies of brown blotch disease in *A. bisporus*.

## Results

### Isolates pathogenicity

Extensive brown blotches have been observed on young and mature fruiting bodies of *A. bisporus* in Guangxi, China (Fig. 1a,b), rendering them completely valueless. The incidence rate of this disease is 10%. Twenty-two strains were isolated from the diseased tissue, and pathogenicity tests confirmed that 16 were pathogenic against *A. bisporus*. Seven pathogenic strains were isolated from brown blotch lesions on young fruiting bodies, including Y60, Y64, Y68, G4, G6, G8, and N17. Nine pathogenic strains were isolated from tissues with extensive brown blotch lesions on mature fruiting bodies, including LC12, LC27, LC28, W1, W2, W5, SHe12, SH36, and SH41. Among them, strains G4, G6, SHe12, W1, W2, W5, LC12, LC27, LC28, Y60, Y64, and Y68 exhibited similar pathogenic symptoms, with obvious browning occurring on the caps of *A. bisporus* after inoculation with bacterial suspension (Fig. 1c). Brown blotches spread outward from the inoculation sites (Fig. 1c), and the severity of browning increased with prolonged inoculation time. Pot experiments also demonstrated that inoculation with the above strains at a concentration of $1 \times 10^8$ CFU/g (soil wet weight) caused extensive brown blotch lesions on the caps of *A. bisporus* (Fig. 1d).

Strains SH36, SH41, G8, and N17 exhibited similar pathogenic symptoms, with distinct brown blotches appearing after inoculation with bacterial suspension (Fig. 1e). The pot pathogenicity test confirmed that SH36, SH41, G8, and N17 can induce brown blotches on *A. bisporus* (Fig. 1f). However, the area of brown blotches caused by these strains was smaller compared to other strains, consistent with the results observed when the bacterial suspension was directly inoculated onto the mushroom caps.

Artificial inoculation produced symptoms identical to those observed at the initial isolation sites, and pathogens were re-isolated from the affected regions. Koch's postulates were completed using 16S rRNA sequencing and morphological identification assays.

### Pathogen identification

All pathogenic strains were identified as Gram-negative bacteria. Based on multigene phylogenetic analysis, strains G4, G6, SHe12, W1, W2, W5, LC12, LC27, LC28,
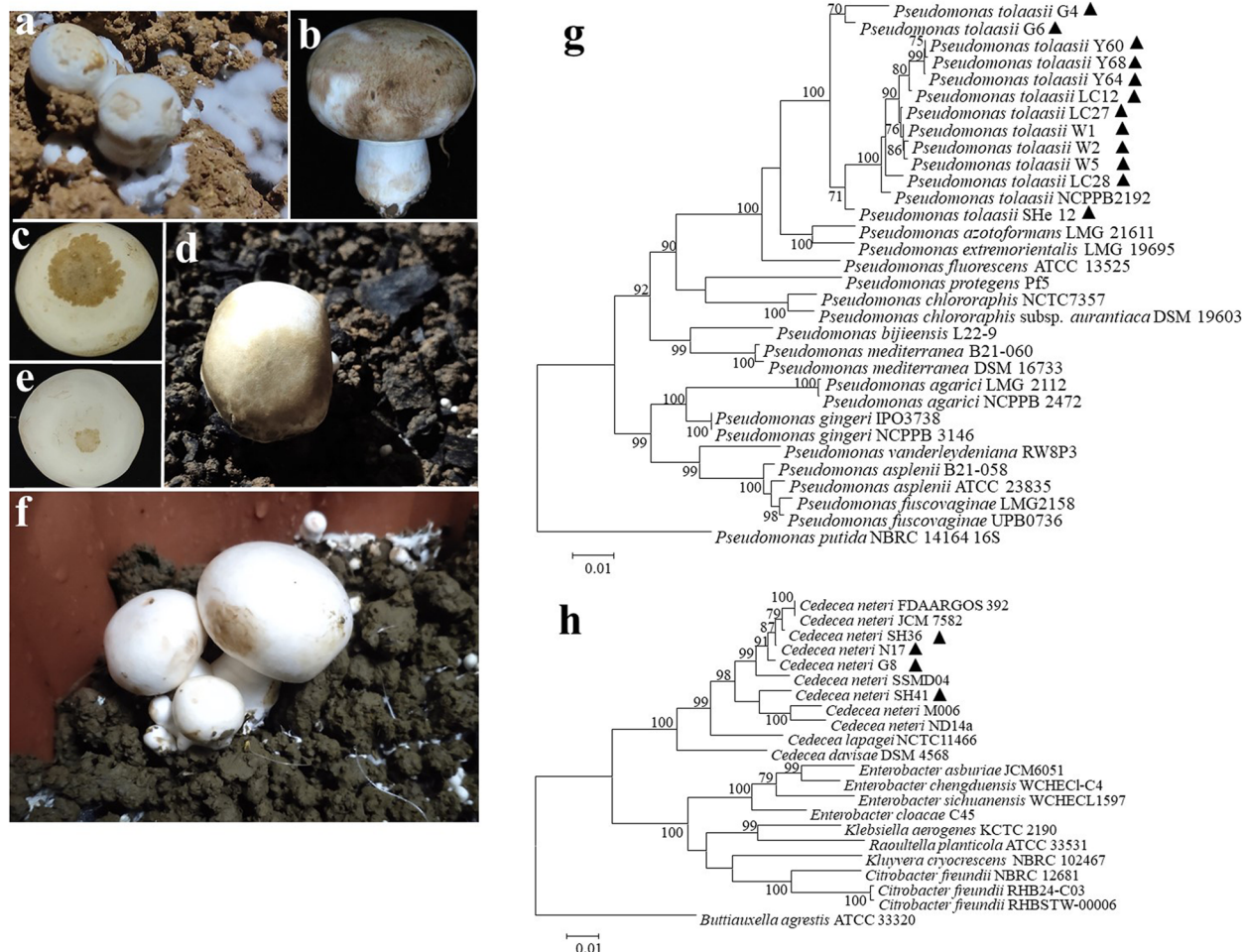
**Fig. 1** Symptoms of natural infection of brown blotch disease in *A. bisporus*, pathogenicity testing, and phylogenetic analysis of the pathogens. **a** Symptoms of natural infection in young fruiting bodies. **b** Symptoms of natural infection in mature fruiting bodies. **c** Symptoms 48 h after inoculation with *P. tolaasii* suspension. **d** Pathogenic symptoms in pot experiments with inoculation of $1 \times 10^8$ CFU/g (soil wet weight) *P. tolaasii*. **e** Symptoms 48 h after inoculation with *C. neteri* suspension. **f** Pathogenic symptoms in pot experiments with inoculation of $1 \times 10^8$ CFU/g (soil wet weight) *C. neteri*. **g** Phylogenetic tree of inter-species relationships within the *Pseudomonas* genus, based on concatenated sequences of 16S rRNA (1–1334 bp), *gapA* (1335–1904 bp), *gltA* (1905–2648 bp), *gyrB* (2649–3085 bp), *recA* (3086–3781 bp), and *rpoB* (3782–4479 bp). **h** Phylogenetic tree of *C. neteri* and closely related species based on concatenated sequences of 16S rRNA (1–1195 bp), *atpD* (1196–2080 bp), *dnaJ* (2081–2700 bp), *tuf* (2701–3033 bp), and *gyrB* (3034–4173 bp). The tree was constructed using the Maximum Likelihood method (ML). ▲ indicates strains isolated in this study

Y60, Y64, and Y68 were grouped with *P. tolaasii* (Fig. 1g). The colonies of these 12 strains on nutrient agar (NA) plates appeared creamy white, circular, moist, raised, smooth, with neat edges and had a diameter of 1–2 mm (Additional file 1: Figure S1a). Cells were grown on King's B medium for 24 h, and yellow fluorescence was observed under UV light (Additional file 1: Figure S1b). The cells were rod-shaped, measuring 1.2–2.0×0.6–1.0 µm, with single polar flagella and no spore (Additional file 1: Figure S1c). They were capable of hydrolyzing arginine, liquefying gelatin, and utilizing citrate, malate, glucose, and arabinose but were unable to utilize sucrose, urea, inosine,

and maltose. Therefore, these 12 strains were identified as *P. tolaasii* based on the results of multigene phylogenetic analysis, morphological characterization, and physiological and biochemical tests.

Strains SH36, SH41, G8, and N17 were grouped with *C. neteri* (Fig. 1h), and their colonies on NA plates appeared oyster white, circular, smooth, raised, with smooth edges, and had a diameter of 1–2 mm (Additional file 1: Figure S1d). Cells were incubated on King's B medium for 24 h, and no fluorescence was observed under UV light (Additional file 1: Figure S1e). The cells were short rods, measuring 1.0–1.5×0.7–1.0 µm, with peritrichous flagella,

and no capsule or spores were observed (Additional file 1: Figure S1f). They were capable of liquefying gelatin, positive for arginine dihydrolase, sucrose, sorbitol, glucose, nitrate reduction, and malate, and negative for arabinose, xylose, urea, lysine, and ornithine. Therefore, these six strains were identified as *C. neteri* based on the results of phylogenetic analysis, morphology, and physiological biochemistry assays.

### Biological characteristics

#### Effect of different temperatures on pathogen growth

Within the temperature range of 22–37 ℃, all pathogenic bacteria exhibited an initial increase followed by a decrease in growth rate (Fig. 2). However, different pathogenic bacteria demonstrated varying optimal growth temperatures, with *P. tolaasii* showing the highest growth rate at 25–28 ℃ and *C. neteri* at 28–30 ℃. The results above indicate that both *P. tolaasii* and *C. neteri* have a wide temperature range for growth, encompassing the temperature range suitable for the growth of *A. bisporus* fruiting bodies.
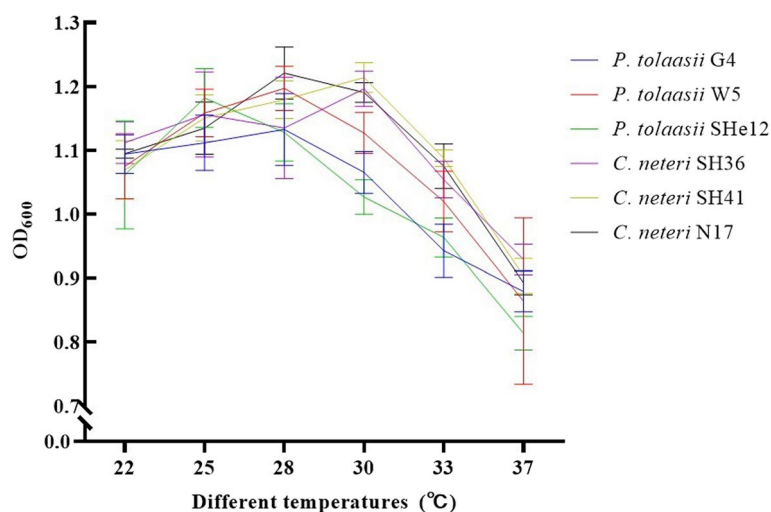
#### Effect of pH on pathogen growth

The effect of pH on the growth of the two pathogens varied. All tested strains of *C. neteri* exhibited good growth at pH 4–9, with the fastest growth observed at pH 5 (Fig. 3). *P. tolaasii* demonstrated growth within the pH range of 5–9, with optimal growth occurring at pH 7–8 (Fig. 3). Neither of the pathogenic bacteria could grow at pH 10. These results demonstrate that these pathogens are capable of rapid proliferation within the pH range suitable for optimal growth of *A. bisporus*.

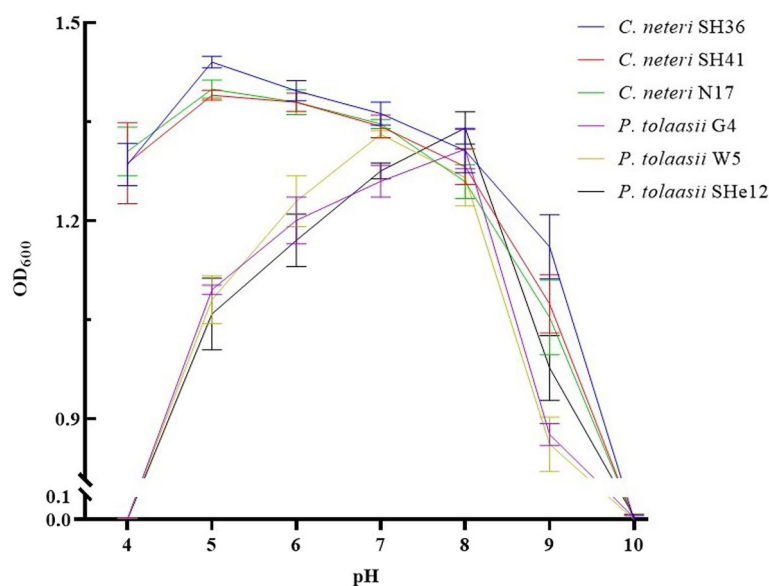#### Swarming and swimming motility test

The swarming and swimming of the pathogenic bacteria are both driven by flagella, which significantly contribute to the size of the disease lesions (Yu et al. 2021). During our observations of pathogen morphology, we found that all pathogens possess flagella, with *P. tolaasii* exhibiting polar flagella and *C. neteri* possessing peritrichous flagella. The results demonstrated that all pathogens exhibited swarming motility, with no significant differences among them (Fig. 4a). However, there was a significant difference in the swimming motility between *P. tolaasii* and *C. neteri* ($P < 0.05$), with *P. tolaasii* cells showing much larger swimming zones compared to *C. neteri* (Fig. 4b).

#### The sodium dodecyl sulfate (SDS) and $H_2O_2$ resistance of pathogens

*P. tolaasii* and *C. neteri* exhibited strong resistance to SDS, displaying rapid growth even in LB medium containing 0.010% SDS (Fig. 5a). *C. neteri* demonstrated stronger SDS resistance than *P. tolaasii*, with all *C. neteri* strains growing faster than *P. tolaasii* under any tested SDS concentrations. This difference was particularly pronounced at SDS concentrations greater than 0.010% (Fig. 5a), indicating that *C. neteri* has stronger SDS resistance than *P. tolaasii*. Regarding resistance to $H_2O_2$, the inhibition zone of $H_2O_2$ on *P. tolaasii* was significantly larger than that on *C. neteri* (Fig. 5b,c), indicating that *P. tolaasii* is highly sensitive to $H_2O_2$, while *C. neteri* is insensitive. These observations suggest that *C. neteri* may have a competitive advantage for survival in adverse environmental conditions.



**Fig. 2** Effect of temperature on the growth of pathogenic bacteria

**Fig. 3** Effect of different pH on pathogen growth
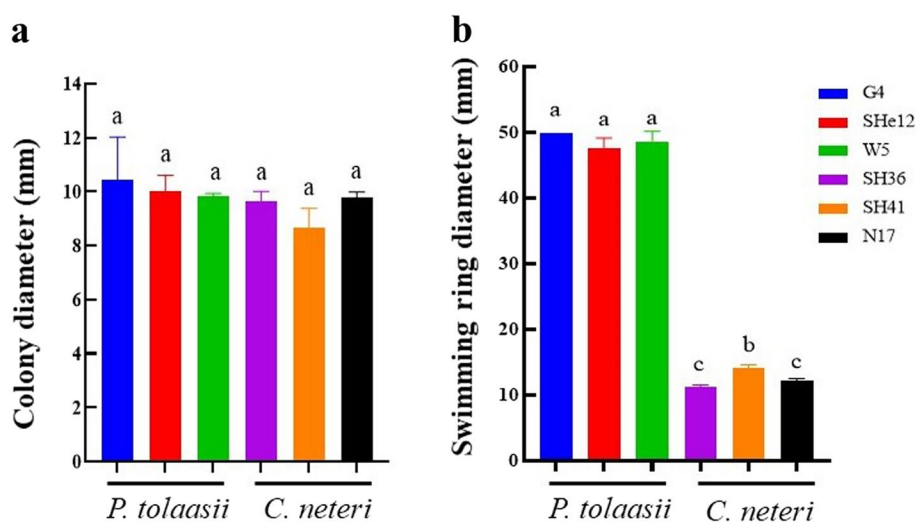


**Fig. 4** The swarming and swimming motility of different pathogens. **a** swarming. **b** swimming. Different lowercase letters indicate statistically significant differences ($P < 0.05$, one-way ANOVA with Duncan's multiple comparisons, $n = 3$)

## Extraction and purification of *C. neteri* toxins

A total of 30.24 g of crude extract in paste form was obtained from 40 L fermentation broth of *C. neteri* SH36. Using petroleum ether/acetone as eluent, 11 fractions (Frs.) were obtained by silica gel column chromatography. Activity assays showed that Fr. 4 (petroleum ether: acetone = 85:15) and 10 (petroleum ether: acetone = 55:45) induced the browning of *A. bisporus*. Fr. 4 and 10 were purified using HPLC under a flow rate of 1.5 mL/min and a detection wavelength of 275 nm.

Compound 1 ($t_R = 11$ min, 36.2 mg) was obtained from Fr.4 using acetonitrile/water (50/50) as the mobile phase, while compound 2 ($t_R = 16$ min, 27.3 mg) was obtained from Fr.10 using acetonitrile/water (35/65) as the mobile phase. Activity assays conducted on compound 1 and 2 demonstrated that inoculating with 60 µg of these compounds caused severe browning of *A. bisporus* after 48 h (Additional file 1: Figure S2). Therefore, it was determined that compounds 1 and 2 were toxins responsible for the browning of *A. bisporus* caused by *C. neteri*.
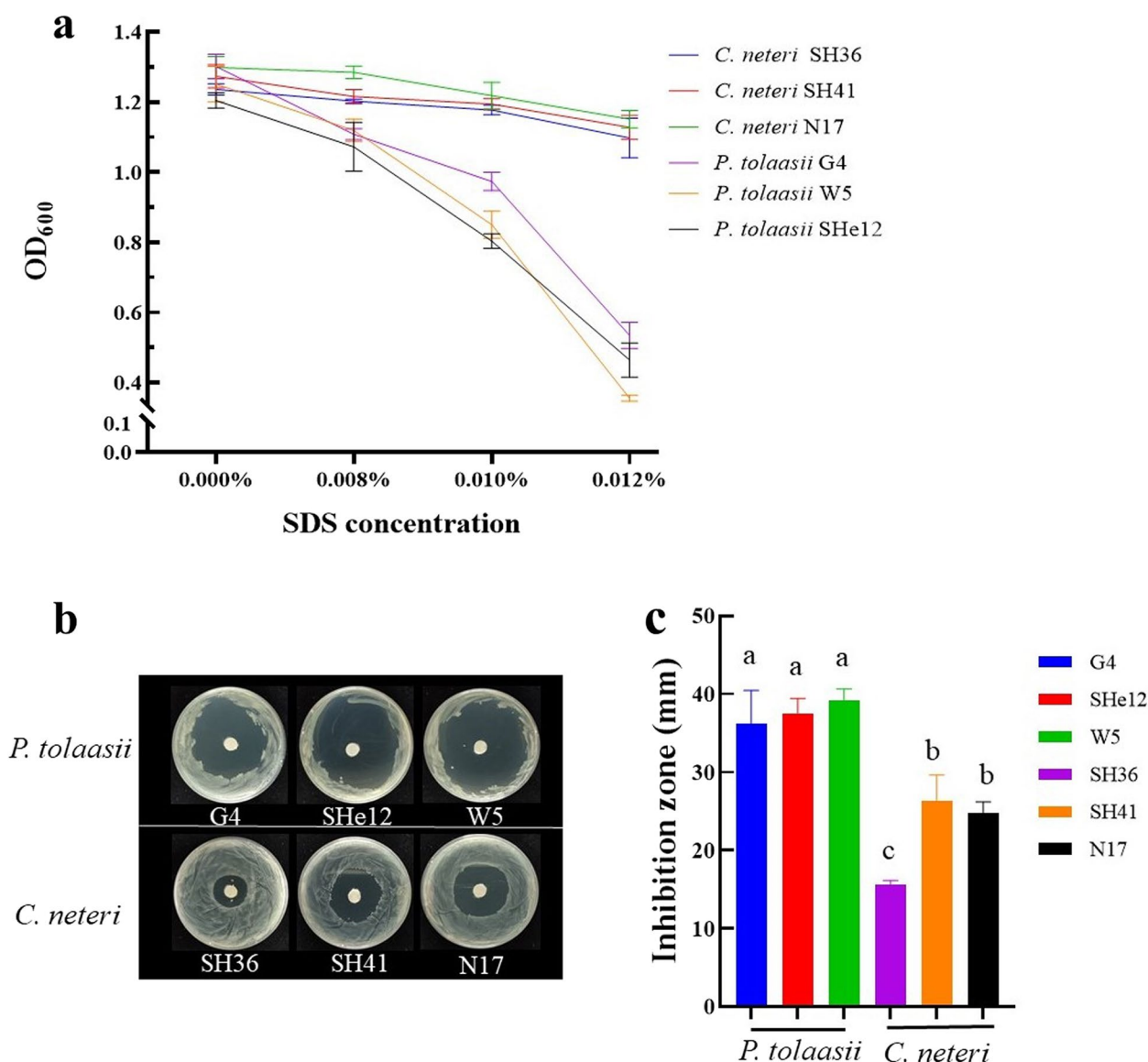
**Fig. 5** The SDS and $H_2O_2$ resistance of different pathogens. **a** Assay of SDS resistance of different pathogens. **b, c** Assay of $H_2O_2$ resistance of different pathogens. Different lowercase letters indicate $P < 0.05$ (one-way ANOVA with Duncan's multiple comparisons, $n = 3$)

## Structure identification of *C. neteri* toxins

Compound 1 (toxin 1) is a colorless powder. ESIMS analysis revealed a protonated ion peak at *m/z* 137 [M + H] + . Its NMR spectra are shown in Additional file 1: Figure S3– 4,: $^{1}$H NMR (600 MHz, DMSO-$d_6$) δ 12.30 (1H, br, s, COOH), 7.34 –7.28 (2H, m, H-3, 5), 7.26 –7.24 (3H, m, H-2,4,6), 3.56 (2H, s, H-7). $^{13}$C NMR (151 MHz, DMSO-$d_6$) δ 172.68 (C-8), 135.02 (C-1), 129.36 (C-2, 6), 128.23 (C-3, 5), 126.57 (C-4), 40.68 (C-7). These data are consistent with those reported by Moore et al. (1997), Fan and Wei (2016), and Wang et al. (2022), identifying the toxin 1 as phenylacetic acid. Its structure is shown in Fig. 6a.

Compound 2 (toxin 2) is a colorless powder. Its protonated ion peak at *m/z* 139 [M + H] + was measured by ESIMS. Its NMR spectra are shown in the Additional file 1: Figure S5–S6: $^{1}$H NMR (600 MHz, DMSO-$d_6$) δ 12.15 (1H, s, COOH), 9.25 (1H, s, OH), 7.06 – 7.00 (2H, m, H-3,5), 6.71 – 6.65 (2H, m, H-2,6). $^{13}$C NMR (151 MHz, DMSO-$d_6$) δ 173.15 (C-7), 156.02(C-4), 130.24(C-2,6), 125.15(C-1), 114.99(C-3,5). These data are consistent with those reported by Tan et al. (2013), Fan and Wei (2016), and Song et al. (2021); therefore, the toxin 2 of *C. neteri* was identified as p-hydroxybenzoic acid. Its structure is shown in Fig. 6b.
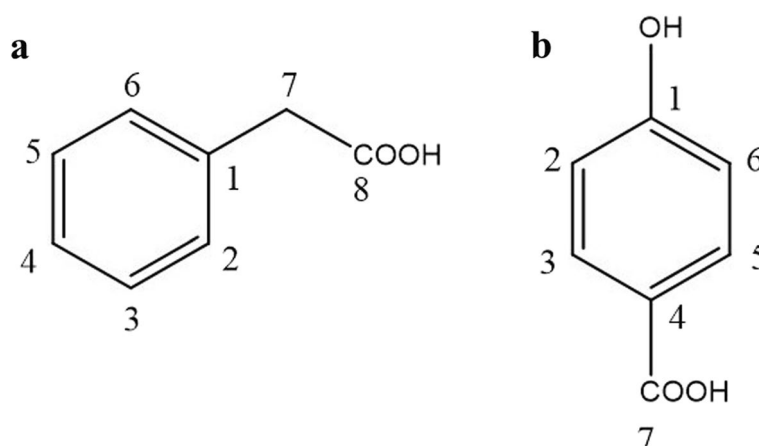
**Fig. 6** The structure of *C. neteri* toxins. **a** The structure of *C. neteri* toxin 1 phenylacetic acid. **b** The structure of *C. neteri* toxin 2 p-hydroxybenzoic acid

## Toxicity of *C. neteri* toxins to *A. bisporus*

The symptoms of *A. bisporus* caused by *C. neteri* toxin 1 (phenylacetic acid) and toxin 2 (p-hydroxybenzoic acid) changed from brown to dark brown with increasing doses (Fig. 7). The toxicity of the two toxins differed in their effects on *A. bisporus*. After inoculation with toxin, p-hydroxybenzoic acid caused distinct brown blotches at 10 µg and severe lesion formation with darker and sunken blotches at 40 µg. Phenylacetic acid caused slight brown discoloration on the *A. bisporus* cap at 10 µg, obvious brown discoloration at 20 µg, and severe lesions with darker blotches at 60 µg. Thus, p-hydroxybenzoic acid exhibits more significant toxicity to *A. bisporus* cap than phenylacetic acid.

We investigated the impact of toxins on tissue colours and measured the whitetness (*L*), red/green (*a*), and yellow/blue (*b*) colour parameters of the inoculated sites of *A. bisporus*. Results showed that phenylacetic acid and p-hydroxybenzoic acid caused significant changes in the values of *L*, *a*, and *b* of *A. bisporus* at 10–60 µg, with *L* value decreasing and *a* value increasing as the concentration of each toxin increased (Fig. 8a–f). This indicates that the two toxins caused a decrease in the whiteness and an increase in the redness of *A. bisporus*. The trend
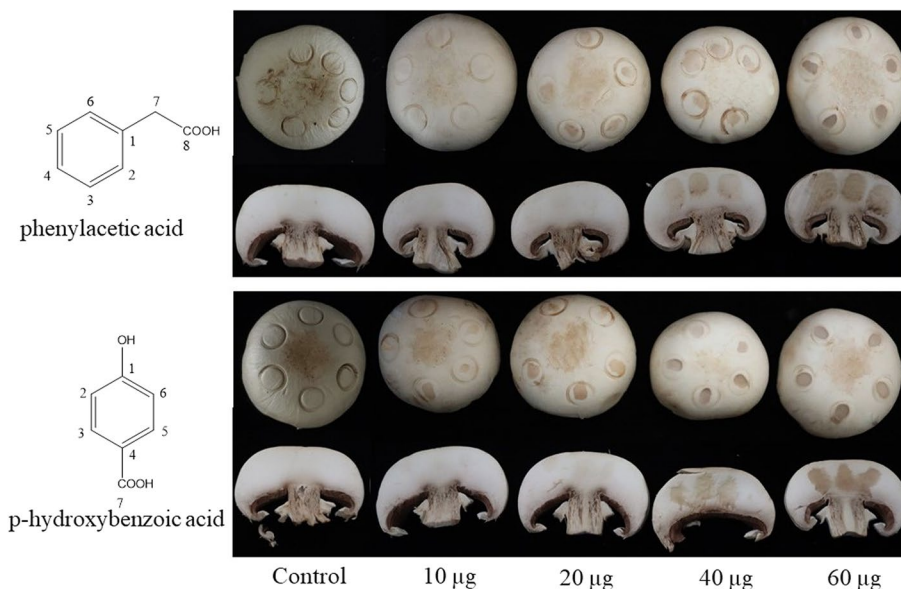


**Fig. 7** Symptoms of *A. bisporus* caused by different concentrations of phenylacetic acid and p-hydroxybenzoic acid. The control is a sterile aqueous solution of 6.5% dimethyl sulfoxide used for dissolving toxins
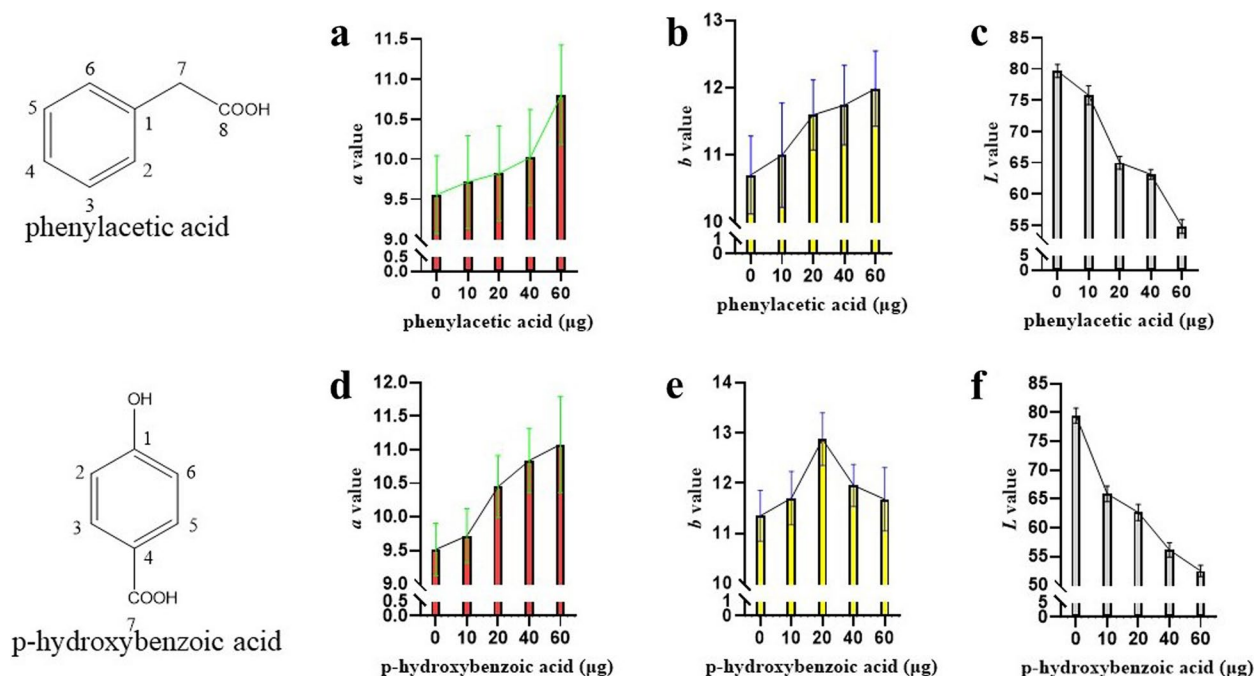
**Fig. 8** Effects of phenylacetic acid and p-hydroxybenzoic acid on color parameters of *A. bisporus*. **a, d** Changes in red/green color parameters (*a*). **b, e** Changes in yellow/blue color parameters (*b*). **c, f** Color parameter lightness (*L*). The *L*, *a*, and *b* values were measured at the toxin-inoculated sites on the *A. bisporus* using a Color Reader. Representative data from three biological replicates are shown as mean ± SD (*n* = 30)

of *b* values affected by phenylacetic acid was consistent with that of *a* values (Fig. 8a, b), and the peak value of *b* was reached at 20 µg for p-hydroxybenzoic acid (Fig. 8e). Further analysis revealed that both toxins caused significant changes in *L* values at all tested concentrations (Additional file 2: Table S1–S2), indicating that the main effect of the two toxins was on the whiteness, leading to the browning of *A. bisporus*. Furthermore, there were differences in the sensitivity to *C. neteri* toxins between *A. bisporus* cap and tissue blocks. The symptoms induced in tissue blocks were less severe than those in caps under the same dose of toxin, and only significant brown discoloration was observed in tissue blocks at 40 µg treatments (Fig. 7).

## Discussion

### *C. neteri* causing *A. bisporus* brown blotch disease in China

In this study, two pathogens, *P. tolaasii* and *C. neteri*, were isolated and identified from brown blotch lesions of *A. bisporus* in China. *P. tolaasii* has been reported as a pathogen causing brown blotch disease in *A. bisporus* worldwide (Osdaghi et al. 2019). *C. neteri* can cause various diseases in edible fungi with a high incidence rate. In recent years, it was found to cause brown blotch disease in *A. bisporus* in Iran, with an incidence rate exceeding 20% (Hamidizade et al. 2022). In China, *C. neteri* has been reported to cause diseases in *Pleurotus pulmonarius*

(Liu et al. 2021), *Pholiota nameko* (Yan et al. 2018), and *Flammulina velutipes* (Yan et al. 2019). However, to our knowledge, this is the first report of brown blotch disease in *A. bisporus* caused by *C. neteri* in China, with a natural incidence rate of 10%. Therefore, *C. neteri* poses a new threat to the cultivation of *A. bisporus*, and more research is needed on its biological characteristics and toxins to better prevent and control this disease.

### Biological characterization of *P. tolaasii* and *C. neteri*

During long-term interactions with pathogens, hosts produce a series of defense responses that are highly detrimental to pathogens. The production of reactive oxygen species is a defense mechanism by hosts to identify pathogen invasion, and $H_2O_2$ plays an important role in this mechanism (Malamud et al. 2012). Sodium dodecyl sulfate (SDS) is often used to evaluate pathogenic bacterial stress-response ability which indirectly reflects their virulence (Lo et al. 2020). In this study, *C. neteri* exhibited stronger resistance to SDS and $H_2O_2$ and had a broader pH adaptation range compared to *P. tolaasii*. Therefore, *C. neteri* is more likely to evade host defense responses, leading to a high incidence rate. Swarming motility is essential in pathogen invasion (Qi et al. 2020; Roy et al. 2022). Hermenau et al. (2020) found that the *P. tolaasii* mutant lacking the *pseB* gene retained its pathogenicity but had much smaller colony sizes and brown

blotch on *A. bisporus*. It has also been demonstrated that *P. tolaasii* mutants lacking tolaasin production still exhibit swarming motility (Henkels et al. 2014). The findings of this study demonstrate that both *P. tolaasii* and *C. neteri* exhibit swarming motility, but the swimming of *P. tolaasii* is significantly stronger compared to *C. neteri*. Moreover, when an equal number of cells were inoculated onto *A. bisporus*, the brown blotches caused by *P. tolaasii* were larger than those induced by *C. neteri*. *Xanthomonas oryzae* pv. *oryzae* strains with strong swimming motility result in larger lesion areas, while loss of swimming motility does not affect their pathogenicity (Yu et al. 2021; Wang et al. 2015). Therefore, the size of brown blotches may be related to the swimming of the pathogens, and this needs to be further confirmed.

### Extraction and structure identification of *C. neteri* toxins

The classical method for discovering microbial natural products involves the isolation and purification of bioactive substances from microbial fermentation media using various chromatographic techniques, followed by structural identification based on detailed analysis of $^1$H NMR, $^{13}$C NMR, and MS data of the target compounds (Schafhauser and Kulik 2022). This approach has been successfully applied in the discovery of pathogenic toxins from pathogens of edible fungi, such as several major toxins from *P. tolaasii*, *P. 'gingeri'*, and *Trichoderma aggressivum* ( Nutkins et al. 1991; Park et al. 1994; Krupke et al. 2003; Bassarello et al. 2004; Huang et al. 2023). In this study, two toxins causing brown blotches on *A. bisporus*, namely phenylacetic acid (0.91 mg/L) and p-hydroxybenzoic acid (0.68 mg/L), were extracted and identified from *C. neteri* fermentation broth using this method. Previous studies have demonstrated that using toxin inhibitors for disease control is a new and effective strategy (Lee et al. 2009; Park et al. 2010; Yun et al. 2023), and this study's results provide a foundation for developing such a strategy.

### The fungal toxicity of *C. neteri* toxins

Phenylacetic acid is a major biocontrol factor of several biocontrol bacteria and exhibits potent antifungal activity (Burkhead et al. 1998; Mao et al. 2006; Wu et al. 2020). It is also an active substance against *Sclerotinia sclerotiorum* in oilseed rape, capable of severely damaging the morphology of *S. sclerotiorum* mycelium (Zhang et al. 2022). Many plants contain endogenous p-hydroxybenzoic acid, which exhibits strong antifungal activity and is an excellent compound for controlling plant fungal diseases (Silva et al. 2020; Xu et al. 2022; Hou et al. 2023). This suggests that phenylacetic acid and p-hydroxybenzoic acid possess broad fungicidal activities. The present study also confirmed that phenylacetic acid and p-hydroxybenzoic acid

can induce browning symptoms in *A. bisporus*. Among them, p-hydroxybenzoic acid exhibits stronger toxicity to *A. bisporus*, causing visible brown blotches at 10 μg and leading to deep brown discoloration and collapse of *A. bisporus* at 40 μg. This is the first report on the extraction of phenylacetic acid and p-hydroxybenzoic acid from the pathogen of edible fungi.

## Conclusions

In conclusion, *A. bisporus* pathogens and their biological characteristics are diverse. *C. neteri* exhibits stronger stress resistance and broader pH adaptability compared to *P. tolaasii*, while *P. tolaasii* demonstrates higher swimming motility than *C. neteri*. The brown blotch disease in *A. bisporus* is induced by *C. neteri* through the production of phenylacetic acid and p-hydroxybenzoic acid. This study is the first report on the comparison of biological characteristics between *P. tolaasii* and *C. neteri*, and the identification of toxins produced by *C. neteri*. These findings provide valuable insights for developing precise prevention and control strategies for brown blotch disease in *A. bisporus*.

## Methods

### Bacterial isolation

Following the method described by Hamidizade et al. (2020), the diseased caps of *A. bisporus* were disinfected with 75% ethanol for 30 s, rinsed three times with sterile water, and air-dried. Approximately $5 \times 5$ mm tissue samples from the diseased area were collected and placed in a 2 mL sterile Eppendorf tube containing 1 mL of sterile water. The tissue was homogenized using a sterile 1 mL pipette tip to create a suspension.

The suspension mentioned above was then serially diluted in sterile water to obtain dilutions of $10^{-1}$, $10^{-2}$, $10^{-3}$, $10^{-4}$, $10^{-5}$, $10^{-6}$, and $10^{-7}$. Each dilution (120 μL) was spread evenly onto Luria–Bertani (LB) (tryptone 10 g/L, yeast extract 5 g/L, NaCl 10 g/L, pH 7.4) agar plates using sterile spreaders, and the plates were incubated at 28 °C for 24 h. Colonies with different colors, shapes, and sizes were selected and purified two to three times on LB agar plates using streaking methods to obtain pure cultures.

### Pathogenicity analysis

The obtained pure cultures were inoculated into LB liquid medium and cultured at 28 °C with a shaking speed of 160 rpm for 16 h. The cultures were centrifuged at 2800 g for 10 min to collect the bacterial cells. The cells were washed twice with sterile water and collected by centrifugation. The resulting bacterial cells were resuspended in sterile water to achieve a concentration of $1.1 \times 10^9$ CFU/mL.

Healthy and uniform-sized young fruiting bodies (with a cap diameter of 2–3 cm) of *A. bisporus* were selected for pathogenicity experiments. Each fruiting body was inoculated with 30 µL of bacterial suspension, and 10 mushrooms were treated with each pathogen. The inoculated mushrooms were placed in a mushroom cultivation room with a temperature of 20 ℃ and a relative humidity of 80–85%. Pathogenicity evaluation was conducted 1–5 days after inoculation.

In the pot pathogenicity experiment, following the method described by Taparia et al. (2020; 2021), the commonly used production strain As 2796 was employed. When the mycelium fully colonized the mushroom cultivation medium in the growth room at 25 ℃, a 4 cm thick casing soil was applied on the surface of the mycelium, and sterile water was used for watering. After incubation at 25 ℃ for 7 d, the temperature was lowered to 18 ℃ while maintaining a relative humidity of 90%. The pathogen suspension was inoculated 5 d later at a concentration of $1 \times 10^8$ CFU/g (soil wet weight), with an equal volume of sterile water used as a control. The occurrence of brown blotches on the mushrooms was then observed.

Bacteria were isolated again from the symptomatic areas, and their morphology and molecular identification were performed to confirm whether they matched the artificially inoculated pathogenic bacteria, thereby verifying Koch's postulates.

### Pathogen identification

Genetic identification of the pathogens was performed using multiple genes. Specifically, the genus was first determined based on the 16S rRNA gene sequence, followed by accurate identification using specific housekeeping genes for the respective genus. Different primers were used to amplify different gene sequences, and the primer information is shown in Additional file 2: Table S3. The PCR reaction system was 25 µL, including 12.5 µL of 2×Rapid Taq Master Mix, 0.5 µL each of the forward and reverse primers, 1 µL of DNA template, and 10.5 µL of ddH$_2$O. The amplification conditions were as follows: initial denaturation at 95 ℃ for 3 min, denaturation at 95 ℃ for 15 s, annealing at 45–58 ℃ for 15 s, extension at 72 ℃ for 30 s, repeated for 34 cycles, and a final extension at 72 ℃ for 5 min. The PCR products were purified by 1% agarose gel electrophoresis, and the sequencing was conducted by BGI Genomics Co., Ltd. The ContigExpress software was used to edit the sequences, and the NCBI online alignment tool BLAST was used to compare them with the GenBank database. Representative sequences of taxonomic groups were selected and downloaded from the database. The amplified sequences from this study have been deposited in the NCBI GenBank database under the accession numbers listed in the Additional file 2: Table S4. The obtained sequences from this study were aligned with the downloaded sequences from the GenBank database using ClustalW in MEGA X software, and a phylogenetic tree was constructed using the maximum likelihood method (ML) with 1000 bootstrap replicates.

The colonies were cultured in nutrient agar (NA) medium (peptone 10 g/L, beef extract 5 g/L, agar 15 g/L, pH 7.3) for 24 h and observed for colony morphology and color under a stereomicroscope. King's B medium (peptone 20 g/L, K$_2$HPO$_4$ 1.5 g/L, MgSO$_4$ 1.5 g/L, agar 15 g/L, pH 7.3) was used to observe the production of fluorescence after 24 h of incubation under UV light. Gram staining was performed using Solarbio Gram staining kit, and the staining results were observed under a 100×oil immersion lens. Cell size and morphology were observed using scanning electron microscopy (JEOL JEM-1400FLASH, Tokyo, Japan). The physiological and biochemical characteristics of the pathogen were tested using Hangzhou Microbial Reagent Co.

### Effect of different temperatures on pathogen growth

An aliquot of 0.5 mL of pathogenic bacterial suspension was inoculated into a 100 mL centrifuge tube containing 50 mL LB medium and placed at 22, 25, 28, 30, 33, and 37 ℃ under shaking at 160 rpm for 24 h. The OD$_{600}$ of the bacterial suspension cultured at each temperature was measured. Three representative strains were selected for each species for the study, and the experiment was repeated three times.

### Effect of pH on pathogen growth

The pH of the culture medium was adjusted to 4, 5, 6, 7, 8, 9, and 10 using 1 mol/L NaOH and HCl. A total of 0.5 mL of pathogenic bacterial suspension was inoculated into 100 mL centrifuge tubes containing 50 mL of LB liquid medium at each of the pH levels mentioned above. The cultures were grown at 28 ℃ with shaking at 160 rpm for 24 h, and the OD$_{600}$ of the bacterial suspensions at each pH level was measured. Three representative strains of each species were selected for study. The experiment was repeated three times.

### Swarming motility test

Following the method described by Yu et al. (2021), An aliquot of 2 µL of pathogenic bacterial suspension was inoculated into a bacterial swarming detection medium (1 g/L tryptone, 0.5 g/L yeast extract, 10 g/L glucose, 1 g/L NaCl, 6 g/L agar) and incubated at 28 ℃ for 48 h. The diameter of the bacterial colonies was measured, and three representative strains of each species were selected for study. The experiment was repeated three times.

Huang *et al. Phytopathology Research*      (2024) 6:21

Page 11 of 13

### Swimming motility test

Using the methods described by Yu et al. (2021) and Lai et al. (2018), a sterile toothpick was used to dip into a pathogenic bacterial suspension and then stabbed into a bacterial motility detection medium (0.3 g/L polypeptone, 0.3 g/L yeast extract, 0.3 g/L agar) at 28 °C for 48 h. The diameter of the bacterial motility circle was measured, and three representative strains of each species were selected for analysis. The experiment was repeated three times.

### Assay of pathogen resistance to sodium dodecyl sulfate (SDS)

Different amounts of SDS were added to the LB medium to achieve final concentrations of 0.008%, 0.010%, and 0.012% (w/v), with no addition of SDS serving as the control. Then, 0.5 mL pathogenic bacterial suspension was inoculated into 50 mL of LB medium containing different concentrations of SDS in a 100 mL centrifuge tube. The tubes were shaken at 160 rpm under 28 °C for 24 h before the $OD_{600}$ of the culture was measured. Three representative strains of each species were selected for study. The experiment was repeated three times.

### The $H_2O_2$ resistance detection of pathogens

An aliquot of 60 μL pathogenic bacterial suspension was evenly spread on a 60 mm LB agar plate. Sterilized filter paper discs (6 mm) were placed at the center of the plate, and 10 μL 30% $H_2O_2$ were added to the filter paper. The plates were incubated at a temperature of 28 °C for 48 h, and the diameter of the inhibition zone was measured. Three representative strains were selected for each species for the study. The experiment was repeated three times.

### Extraction, purification, and structural identification of *C. neteri* toxins

Following the previous method (Huang et al. 2023), the ethyl acetate (EA) extract was obtained from the deep fermentation broth (cultured for 4 days) of *C. neteri*. The EA extract was dissolved in a small amount of methanol and mixed with silica gel powder (200–300 mesh) at a ratio of 1.2 times the weight of EA extract. The weight of silica gel powder used for column chromatography was 50 times the weight of EA extract. The separation system consisted of petroleum ether:acetone = 100:0 ~ 40:60, with an incremental increase of acetone by 5% each step. Each gradient elution volume was 1.5 L, 150 mL was collected as one fraction, and fractions with similar components were combined based on thin-layer chromatography (GF254, 40 μm; Qingdao Marine Chemical Factory) results. Each fraction was diluted in 6.5% DMSO (3 mg/mL) and subjected to activity screening, and fractions showing activity were further purified using high-performance liquid chromatography (HPLC).

The toxin (5.0 mg) was dissolved in 600 μL of deuterated dimethyl sulfoxide (DMSO-$d_6$). The toxin's nuclear magnetic resonance (NMR) spectra were obtained using a Bruker AVANCE III HD 600 spectrometer, specifically acquiring ^{1}H NMR and ^{13}C NMR spectra at 600 MHz and 151 MHz, respectively. The mass spectrum of the toxin was acquired using a Bruker MiXis TOF-QII mass spectrometer (Bruker, Billerica, MA, USA) (Huang et al. 2023). The toxin's structure was determined based on a detailed analysis of its ^{1}H NMR and ^{13}C NMR spectra data and comparison with relevant literature.

### Toxicity assays of *C. neteri* toxins to *A. bisporus*

Following the methods described by Henkels et al. (2014) and Huang et al. (2023), the toxin was dissolved in 6.5% dimethyl sulfoxide (DMSO) to prepare a toxin stock solution with a concentration of 10 mg/mL. The stock solution was then diluted to 500, 1000, 2000, and 3000 μg/mL. For each concentration, 20 μL of the solution was inoculated onto the depilated caps of *A. bisporus*, with 6 mushrooms per treatment. The site of toxin inoculation was gently pressed using a sterile 1 mL pipette tip. A corresponding solvent was used as a negative control. The treated *A. bisporus* were placed in sterile culture dishes and incubated at 20°C with 85% humidity. After 48 h, the observations were recorded and photographs were taken. The brightness parameters (*L*), red/green color parameters (*a*), and yellow/blue color parameters (*b*) of the inoculated sites were measured using a Color Reader (KONICA MINOLTA).

### Data analysis

All data were based on the mean values of at least three biological replicates, and all data were presented as mean ± standard deviation. One-way analysis of variance (ANOVA) was performed using SPSS27, and different letters indicate statistically significant differences at $P < 0.05$. The graphs were created using GraphPad Prism 8.

### Abbreviations

| | |
|---|---|
| ANOVA | Analysis of variance |
| CFU | Colony forming units |
| DMSO | Dimethyl sulfoxide |
| EA | Ethyl acetate |
| Fr | Fraction |
| HPLC | High-performance liquid chromatography |
| LB | Luria-bertani |
| ML | Maximum likelihood |
| MLST | Multilocus sequence typing |
| MS | Mass spectrometry |
| NA | Nutrient agar |
| NCBI | National center for biotechnology information |
| NMR | Nuclear magnetic resonance |
| rpm | Revolutions per minute |

Huang *et al. Phytopathology Research*      (2024) 6:21

Page 12 of 13

| SDS | Sodium dodecyl sulfate |
| SGCC | Silica gel column chromatography |
| TIFs | Tolaasin-inhibitory factors |
| TLC | Thin-layer chromatography |
| UV | Ultraviolet |

## Supplementary Information

The online version contains supplementary material available at https://doi.org/10.1186/s42483-024-00239-8.

---

**Additional file 1: Figure S1.** Morphological identification of pathogens. **Figure S2.** Compound 1 and compound 2 caused severe brown discoloration of *A. bisporus*. **Figure. S3** The $^1$H NMR spectrum of *Cedecea neteri* toxin 1 in DMSO. **Figure S4.** The $^{13}$C NMR spectrum of *Cedecea neteri* toxin 1 in DMSO. **Figure S5.** The $^1$H NMR spectrum of *Cedecea neteri* toxin 2 in DMSO. **Figure S6.** The $^{13}$C NMR spectrum of *Cedecea neteri* toxin 2 in DMSO.

**Additional file 2: Table S1.** Effect of different concentrations phenylacetic acid on the *L*, *a*, and *b* value of the *A. bisporus* caps. **Table S2.** Effect of different concentrations p-hydroxybenzoic acid on the *L*, *a*, and *b* value of the *A. bisporus* caps. **Table S3.** Multilocus sequence typing (MLST) primers**. Table S4.** NCBI GenBank accession numbers of the sequences amplified in this study.

---

## Availability of data and materials
 The datasets used and/or analyzed during the current study are available from the corresponding author on reasonable request.

## Declarations

### Ethics approval and consent to participate
Not applicable.

### Consent for publication
Not applicable.

### Competing interests
The authors declare that they have no competing financial interests or personal relationships that may have influenced the work reported in this study.

## References

Bassarello C, Lazzaroni S, Bifulco G, Lo Cantore P, Iacobellis NS, Riccio R, et al. Tolaasins A– E, five new lipodepsipeptides produced by *Pseudomonas tolaasii*. J Nat Prod. 2004;67(5):811–6. https://doi.org/10.1021/np0303557.

Burkhead KD, Slininger PJ, Schisler DA. Biological control bacterium Enterobacter cloacae S11: T: 07 (NRRL B-21050) produces the antifungal compound phenylacetic acid in Sabouraud maltose broth culture. Soil Biol Biochem. 1998;30(5):665–7. https://doi.org/10.1016/S0038-0717(97)00170-3.

Cantore PL, Iacobellis NS. First report of brown discoloration of *Agaricus bisporus* caused by *Pseudomonas agarici* in southern Italy. Phytopathol Mediterr. 2004;43(1):35–8. https://doi.org/10.14601/Phytopathol_Mediterr-1731.

Fan L, Wei XH. Metabolites of endolichenic bacteria *Methylobacterium* sp. Chin J Antibiot. 2016;41(07):520–3. https://doi.org/10.13461/j.cnki.cja.005778.

Hamidizade M, Taghavi SM, Martins SJ, Herschlag RA, Hockett KL, Bull CT, et al. Bacterial brown pit, a new disease of edible mushrooms caused by *Mycetocola* sp. Plant Dis. 2020;104(5):1445–54. https://doi.org/10.1094/PDIS-10-19-2176-RE.

Hamidizade M, Taghavi SM, Mafakheri H, Herschlag RA, Martins SJ, Hockett KL, et al. First report of brown spot on white button mushroom (*Agaricus bisporus*) caused by *Cedecea neteri* in Iran. Plant Dis. 2022;106(4):1291. https://doi.org/10.1094/PDIS-06-21-1305-PDN.

Henkels MD, Kidarsa TA, Shaffer BT, Goebel NC, Burlinson P, Mavrodi DV, et al. *Pseudomonas protegens* Pf-5 causes discoloration and pitting of mushroom caps due to the production of antifungal metabolites. Mol Plant Microbe Interact. 2014;27:733–46. https://doi.org/10.1094/MPMI-10-13-0311-R.

Hermenau R, Kugel S, Komor AJ, Hertweck C. Helper bacteria halt and disarm mushroom pathogens by linearizing structurally diverse cyclolipopeptides. PNAS. 2020;117(38):23802–6. https://doi.org/10.1073/pnas.2006109117.

Hou XL, Luo CQ, Chen SS, Zhang XW, Jiang JM, Yang ZF, et al. Progress in research on diseases of edible fungi and their detection methods: a review. Crop Prot. 2023;174:106420. https://doi.org/10.1016/j.cropro.2023.106420.

Huang ZX, Liang XS, Wang YF, Mo MQ, Qiu Y, Liu B. Ginger blotches on *Agaricus bisporus* due to monoacetylphloroglucinol production by the pathogen *Pseudomonas 'gingeri'*. Pest Manag Sci. 2023;79(12):5197–207. https://doi.org/10.1002/ps.7725.

Krupke OA, Castle AJ, Rinker DL. The North American mushroom competitor, Trichoderma aggressivum f. aggressivum, produces antifungal compounds in mushroom compost that inhibit mycelial growth of the commercial mushroom Agaricus bisporus. Mycol Res. 2003;107(12):1467–75. https://doi.org/10.1017/S0953756203008621.

Lai JL, Tang DJ, Liang YW, Zhang R, Chen Q, Qin ZP, et al. The RNA chaperone Hfq is important for the virulence, motility and stress tolerance in the phytopathogen *Xanthomonas campestris*. Environ Microbiol Rep. 2018;10(5):542–54. https://doi.org/10.1111/1758-2229.12657.

Lee Y, Woo Y, Lee S, Kang K, Yong Y, Kim JK, et al. Identification of compounds exhibiting inhibitory activity toward the *Pseudomonas tolaasii* toxin tolaasin I using in silico docking calculations, NMR binding assays, and in vitro hemolytic activity assays. Bioorganic Med Chem Lett. 2009;19:4321–4. https://doi.org/10.1016/j.bmcl.2009.05.068.

Liu ZL, Zhou SY, Zhang WL, Wu SJ, Chen XF, Wang XG, et al. First report of *Cedecea neteri* causing yellow rot disease in *Pleurotus pulmonarius* in China. Plant Dis. 2021;105(4):1189. https://doi.org/10.1094/PDIS-09-20-1886-PDN.

Lo HH, Liao CT, Li CE, Chiang YC, Hsiao YM. The clpX gene plays an important role in bacterial attachment, stress tolerance, and virulence in Xanthomonas campestris pv. campestris. Arch Microbiol. 2020;202:597–607. https://doi.org/10.1007/s00203-019-01772-3.

Malamud F, Conforte VP, Rigano LA, Castagnaro AP, Marano MR, Morais do Amaral A, et al. Hrp M is involved in glucan biosynthesis, biofilm formation and pathogenicity in Xanthomonas citri ssp. citri. Mol Plant Pathol. 2012;13(9):1010–8. https://doi.org/10.1111/j.1364-3703.2012.00809.x.

Mao S, Lee SJ, Hwangbo H, Kim YW, Park KH, Cha GS, et al. Isolation and characterization of antifungal substances from Burkholderia sp. culture broth. Curr Microbiol. 2006;53:358–64. https://doi.org/10.1007/s00284-005-0333-2.

Mleczek M, Budka A, Siwulski M, Mleczek P, Gąsecka M, Jasińska A, et al. Investigation of differentiation of metal contents of *Agaricus bisporus*, *Lentinula edodes* and *Pleurotus ostreatus* sold commercially in Poland between 2009 and 2017. J Food Compost Anal. 2020;90:103488. https://doi.org/10.1016/j.jfca.2020.103488.

Moore BS, Walker K, Tornus I, Handa S, Poralla K, Floss HG. Biosynthetic studies of ω-cycloheptyl fatty acids in Alicyclobacillus cycloheptanicus.

Huang *et al. Phytopathology Research*     (2024) 6:21

Page 13 of 13

Formation of cycloheptanecarboxylic acid from phenylacetic acid. J Org Chem. 1997;62(7):2173–85. https://doi.org/10.1021/jo962402o.

Nutkins JC, Mortishire-Smith RJ, Packman LC, Brodey CL, Rainey PB, Johnstone K, et al. Structure determination of tolaasin, an extracellular lipodepsipeptide produced by the mushroom pathogen *Pseudomonas tolaasii* Paine. J Am Chem Soc. 1991;113:2621–7. https://doi.org/10.1021/ja00007a040.

Osdaghi E, Martins SJ, Ramos-Sepulveda L, Vieira FR, Pecchia JA, Beyer DM, et al. 100 years since tolaas: bacterial blotch of mushrooms in the 21st century. Plant Dis. 2019;103(11):2714–32. https://doi.org/10.1094/PDIS-03-19-0589-FE.

Park CJ, Oh SK, Chun UH. Identification of mushroom brown blotch causing agent from *Pseudomonas tolaasii* culture broth. Appl Biol Chem. 1994;37:392–6.

Park SW, Kim MH, Kim YK. Effects of Tolaasin inhibitory factors on Tolaasin-induced blotch formation and hemolysis. Biophys J. 2010;98:108a. https://doi.org/10.1016/j.bpj.12.599.

Qi YH, Huang L, Liu GF, Leng M, Lu GT. PilG and PilH antagonistically control flagellum-dependent and pili-dependent motility in the phytopathogen Xanthomonas campestris pv. campestris. BMC Microbiol. 2020;20(1):1–14. https://doi.org/10.1186/s12866-020-1712-3.

Ramos M, Burgos N, Barnard A, Evans G, Preece J, Graz M, et al. *Agaricus bisporus* and its by-products as a source of valuable extracts and bioactive compounds. Food Chem. 2019;292:176–87. https://doi.org/10.1016/j.foodchem.2019.04.035.

Roy S, Mittal P, Tayi L, Bondada S, Ray MK, Patel HK, et al. Xanthomonas oryzae pv. oryzae Exoribonuclease R is required for complete virulence in rice, optimal motility, and growth under stress. Phytopathology®. 2022;112(3):501–10. https://doi.org/10.1094/PHYTO-07-21-0310-R.

Schafhauser T, Kulik A. Isolation and purification of natural products from microbial cultures. Antibiotics: methods and protocols. Springer, US, 2022; pp. 75–96.

Sharkady SM, Bailey B, Thompson DK. Characterization of two novel AmpC beta-lactamases from the emerging opportunistic pathogen, Cedecea neteri. Antibiotics. 2023;12(2):219. https://doi.org/10.3390/antibiotics12020219.

Silva B, Souza MM, Badiale-Furlong E. Antioxidant and antifungal activity of phenolic compounds and their relation to aflatoxin B1 occurrence in soybeans (Glycine max L.). J Sci Food Agric. 2020;100(3):1256–64. https://doi.org/10.1002/jsfa.10137.

Soler-Rivas C, Jolivet S, Arpin N, Olivier JM, Wichers HJ. Biochemical and physiological aspects of brown blotch disease of *Agaricus bisporus*. FEMS Microbiol Rev. 1999;23(5):591–614. https://doi.org/10.1111/j.1574-6976.1999.tb00415.x.

Song HZ, Wang J, Yang T, Hou DB, Yuan XH, Li YG. Secondary metabolites from fungus *Chaetomium virescens* CIB608 and their antimicrobial activity. Chin J Appl Environ Biol. 2021;27(04):1078–84. https://doi.org/10.19675/j.cnki.1006-687x.2021.01033.

Tajalipour S, Hassanzadeh N, Khabbaz Jolfaee H, Heydari A, Ghasemi A. Biological control of mushroom brown blotch disease using antagonistic bacteria. Biocontrol Sci Technol. 2014;24(4):473–84. https://doi.org/10.1080/09583157.2013.873113.

Tan D, Yan Q, Kang H. Chemical constituents from *Blumea balsamifera*. Chem Nat Compounds. 2013;48(6):1072–3. https://doi.org/10.1007/s10600-013-0468-5.

Taparia T, Krijger M, Haynes E, Elphinstone JG, Noble R, Van Der Wolf J. Molecular characterization of Pseudomonas from *Agaricus bisporus* caps reveal novel blotch pathogens in Western Europe. BMC Genomics. 2020;21(1):505. https://doi.org/10.1186/s12864-020-06905-3.

Taparia T, Hendrix E, Hendriks M, Krijger M, De Boer W, Van der Wolf J. Comparative studies on the disease prevalence and population dynamics of ginger blotch and brown blotch pathogens of button mushrooms. Plant Dis. 2021;105(3):542. https://doi.org/10.1094/PDIS-06-20-1260-RE.

Thompson DK, Sharkady SM. Genomic insights into drug resistance determinants in *Cedecea neteri*, a rare opportunistic pathogen. Microorganisms. 2021;9(8):1741. https://doi.org/10.3390/microorganisms9081741.

Wang SZ, Sun Z, Wang HQ, Liu LJ, Lu F, Yang J, et al. Rice OsFLS2- mediated perception of bacterial flagellins is evaded by Xanthomonas oryzae pv. oryzae and oryzicola. Mol Plant. 2015;8:1024–37. https://doi.org/10.1016/j.molp.2015.01.012.

Wang R, Guo ZK, Cheng F, Feng QY, Zhan XF. Study on the chemical components produced by the marine Streptomyces sp rssa1 from the South China sea. Nat Prod Res Develop. 2022;34(06):975–80. https://doi.org/10.16333/j.1001-6880.2022.6.009.

Wu JJ, Huang JW, Deng WL. Phenylacetic acid and methylphenyl acetate from the biocontrol bacterium Bacillus mycoides BM02 suppress spore germination in Fusarium oxysporum f. sp. lycopersici. Front Microbiol. 2020;11:569263. https://doi.org/10.3389/fmicb.2020.569263.

Xu HF, Wang GF, Zhang J, Zhang MJ, Fu MR, Xiang K, et al. Identification of phenolic compounds and active antifungal ingredients of walnut in response to anthracnose (*Colletotrichum gloeosporioides*). Postharvest Biol Technol. 2022;192:112019. https://doi.org/10.1016/j.postharvbio.2022.112019.

Yan JJ, Chen BZ, Wang RQ, Liu F, Wei Q, Xie BG, et al. First report of *Cedecea neteri*-induced soft rot disease of *Pholiota nameko* in China. Plant Dis. 2018;102(10):2025–2025. https://doi.org/10.1094/PDIS-12-17-1951-PDN.

Yan JJ, Liu YY, Wang RQ, Mukhtar I, Liu F, Lin ZY, et al. First report of *Cedecea neteri* causing yellow sticky disease in *Flammulina velutipes* in China. Plant Dis. 2019;103(5):1014. https://doi.org/10.1094/PDIS-06-18-1039-PDN.

Yu C, Nguyen DP, Yang FH, Shi J, Wei YM, Tian F, et al. Transcriptome analysis revealed overlapping and special regulatory roles of RpoN1 and RpoN2 in motility, virulence, and growth of Xanthomonas oryzae pv. oryzae. Front Microbiol. 2021;12:653354. https://doi.org/10.3389/fmicb.2021.653354.

Yuan WF, Ruan S, Qi GF, Wang R, Zhao XY. Plant growth-promoting and antibacterial activities of cultivable bacteria alive in tobacco field against *Ralstonia solanacearum*. Environ Microbiol. 2022;24(3):1411–29. https://doi.org/10.1111/1462-2920.15868.

Yun YB, Kim MH, Han JH, Kim YK. Suppression of brown blotch disease by tolaasin inhibitory factors. J Appl Biolog Chem. 2017;60(2):179–84. https://doi.org/10.3839/JABC.2017.029.

Yun YB, Cho KH, Kim YK. Inhibition of Tolaasin cytotoxicity causing brown blotch disease in cultivated mushrooms using Tolaasin inhibitory factors. Toxins. 2023;15(1):66. https://doi.org/10.3390/toxins15010066.

Zhang H, Cheng Q, Wang X, Jia W, Xie JT, Fan GC, et al. Selenium Improved phenylacetic acid content in oilseed rape and thus enhanced the prevention of Sclerotinia sclerotiorum by dimethachlon. J Fungi. 2022;8(11):1193. https://doi.org/10.3390/jof8111193.